Structural and Morphological Characterization of Ultralente Insulin Crystals by Atomic Force Microscopy: Evidence of Hydrophobically Driven Assembly

Christopher M. Yip,* Michael R. DeFelippis,* Bruce H. Frank,* Mark L. Brader,* and Michael D. Ward#
*Lilly Research Laboratories, Eli Lilly and Company, Indianapolis, Indiana 46285, and #Department of Chemical Engineering and Materials Science and the Center for Interfacial Engineering, University of Minnesota, Minneapolis, Minnesota 55455 USA

ABSTRACT Although x-ray crystal structures exist for many forms of insulin, the hormone involved in glucose metabolism and used in the treatment of diabetes, x-ray structural characterization of therapeutically important long-acting crystalline ultralente insulin forms has been elusive because of small crystal size and poor diffraction characteristics. We describe tapping-mode atomic force microscopy (TMAFM) studies, performed directly in crystallization liquor, of ultralente crystals prepared from bovine, human, and porcine insulins. Lattice images obtained from direct imaging of crystal planes are consistent with R3 space group symmetry for each insulin type, but the morphology of the human and porcine crystals observed by AFM differs substantially from that of the bovine insulin crystals. Human and porcine ultralente crystals exhibited large, molecularly flat (001) faces consisting of hexagonal arrays of close packed hexamers. In contrast, bovine ultralente crystals predominantly exhibited faces with cylindrical features assignable to close-packed stacks of insulin hexamers laying in-plane, consistent with the packing motif of the (010) and (011) planes. This behavior is attributed to a twofold increase in the hydrophobic character of the upper and lower surfaces of the donut-shaped insulin hexamer in bovine insulin compared to its human and porcine counterparts that results from minor sequence differences between these insulins. The increased hydrophobicity of these surfaces can promote hexamer-hexamer stacking in precrystalline aggregates or enhance attachment of single hexamers along the *c* axis at the crystal surface during crystal growth. Both events lead to enhanced growth of {hk0} planes instead of (001). The insulin hexamers on the (010) and (110) faces are exposed "edge-on" to the aqueous medium, such that solvent access to the center of the hexamer and to solvent channels is reduced compared to the (001) surface, consistent with the slower dissolution and reputed unique basal activity of bovine ultralente insulin. These observations demonstrate that subtle variations in amino acid sequence can dramatically affect the interfacial structure of crystalline proteins.

INTRODUCTION

Insulin is a 5808-Da, 51 amino acid, dual-chain hormone that is secreted and stored in pancreatic β-cells. It has a significant history, owing to its therapeutic importance for the treatment of diabetes, a chronic disease that often requires supplemental insulin delivered by subcutaneous injection of either solution or microcrystalline suspension formulations (Haycock, 1983). The pharmacokinetics of such therapies are dictated to a large extent by dissociation of the insulin zinc-hexamer to the bioactive monomer (Hollenberg, 1990; Gammeltoft, 1988; Berson and Yalow, 1966; Smith et al., 1984). The therapeutic efficacy of microcrystalline insulin suspensions also may be influenced by the rate of hexamer dissociation from the crystal lattice, which would depend upon the cohesive energy between insulin hexamers, crystal morphology, the dissolution rates of different crystal faces, and the degree of disorder at the crystal-solution interface.

First prepared by Schlichtkrull, crystalline ultralente insulin is a commercially available, long-acting insulin preparation (Hallas-Møller et al., 1952; Schlichtkrull, 1956). Remarkably, despite its long history, this form has defied high-resolution structural analysis, owing to poor diffraction characteristics and small crystal dimensions. The lack of molecular-level structural characterization of ultralente crystals has hampered efforts to design more effective basal insulin preparations and has precluded understanding of the subtle yet therapeutically important differences in the pharmacokinetic characteristics of bovine, human, and porcine ultralente insulin (Galloway and Chance, 1994). Crystalline bovine ultralente insulin—which differs from human and porcine insulins by two residues in the A-chain—is reputed to provide optimal pharmacokinetics with a relatively constant plasma insulin concentration, mimicking that present in nondiabetic individuals. However, it remains unclear how the pharmacokinetics, governed by the dissolution of the microcrystals and insulin monomer absorption into the bloodstream, is related to factors such as the conformation of individual insulin molecules, hexamer packing in the solid state, and crystal morphology (Graham and Pomeroy, 1984). Furthermore, little is known about the role of the

Received for publication 6 April 1998 and in final form 19 June 1998.

Address reprint requests to Dr. Mark L. Brader, Lilly Research Laboratories, Eli Lilly and Company, Indianapolis, IN 46285. Tel.: 317-277-1571; E-mail: brader_mark_l@lilly.com; or to Prof. Michael D. Ward, Department of Chemical Engineering and Materials Science, University of Minnesota, 421 Washington Ave SE, Minneapolis, MN 55455. Tel.: 612-625-3062; Fax: 612-626-7246; E-mail: wardx004@maroon.tc.umn.edu.

Dr. Yip's present address is Department of Chemical Engineering and Applied Chemistry, Institute of Biomedical Engineering, University of Toronto, Toronto, Ontario M5S 3G9, Canada.

0006-3495/98/09/1172/08 $2.00

aforementioned sequence differences on crystal dissociation or growth.

We recently reported that insulin polymorphs, the structure of specific crystal faces, and the influence of sequence modifications on insulin crystal growth and interfacial structure could be characterized directly by in situ atomic force microscopy (AFM) (Yip et al., 1996, 1998). These studies have added to the emergence of AFM as an ideal technique for characterizing the crystal-solution interface and elucidating crystal growth and dissolution processes of small molecule crystals (Mao et al., 1997; Last and Ward, 1996; Hillier and Ward., 1994; Hillier et al., 1994; Carter et al., 1994) and protein crystals (Kuznetsov et al., 1997; Malkin et al., 1995, 1996; Land et al., 1995, 1996; McPherson et al., 1996; Walz et al., 1996; Konnert et al., 1994; Durbin et al., 1992, 1993). AFM is also particularly well suited to the analysis of two-dimensional protein arrays (Muller et al., 1997; Walz et al., 1996; Schabert et al., 1995; Lyon et al., 1993).

These capabilities and the lack of structural characterization of the therapeutically important ultralente insulins prompted us to study microcrystals of these forms by AFM. A previous study in our laboratories of an insulin analog that differed from native human insulin by an inversion of lysyl and prolyl residues at positions 28 and 29 in the B chain demonstrated that this minor sequence change affected crystal growth characteristics and lattice defects in a manner that reflected reduced cohesive energy between hexamers (Yip et al., 1998). This suggests that the sequence difference between bovine and human/porcine insulins may affect the interfacial structure of ultralente crystals, which can be probed directly with AFM. We describe herein the structural characterization of specific crystal faces of ultralente crystals by in situ AFM. Lattice images indicate that each type crystallizes in the R3 space group, but bovine ultralente insulin exhibits a crystal morphology that differs substantially from that of the human and porcine insulins. This is attributed to a greater hydrophobicity on critical external surfaces of the bovine insulin hexamers that favors hexamer-hexamer association into close-packed stacks along the *c* axis rather than the lateral hexamer-hexamer association into (001) layers observed for human and porcine insulins. The morphology observed for bovine ultralente and the close-packed nature of the exposed planes suggest that its unique pharmacokinetics is due to inhibited solvent ingress and reduced dissolution rates compared to the human and porcine forms.

MATERIALS AND METHODS

Crystallization

Single crystals of ultralente insulin were prepared from wild-type bovine, porcine, and recombinant human insulins (Eli Lilly and Company) by batch crystallization (Schlichtkrull, 1956). To a precleaned 20-ml glass scintillation vial containing 30 mg of insulin was added 3 ml of 0.02 M HCl. After gentle swirling to dissolve the insulin, 24 μl aqueous 12 weight % $ZnCl_2$, 0.36 g NaCl, and 2 ml of 0.2 M sodium citrate buffer were added sequentially to afford a slightly turbid solution. The pH of the crystallization liquor was adjusted to 6.25 with dilute sodium hydroxide, and the ensuing clear solution was allowed to stand at room temperature.

Atomic force microscopy

All images were acquired in solution on a Digital Instruments Nanoscope IIIA MultiMode scanning probe microscope (Digital Instruments, Santa Barbara, CA), using a combination contact/tapping mode liquid cell fitted with 120-μm oxide-sharpened silicon nitride V-shaped cantilevers with integral bipyramidal tips (Type DNP-S; Digital Instruments). Before use, the AFM tips were exposed to UV radiation to remove adventitious organic contaminants from the tip surface. Tapping-mode operation in solution employs cantilevers with a lower spring constant than typically are used for tapping mode in air, to compensate for viscous coupling between the tip and surrounding fluid, which effectively raises the cantilever spring constant. Optimal tapping-mode imaging was achieved at frequencies near 8.9 kHz, although we note that selection of the appropriate drive frequency can be influenced by the particular cantilever in use, the sample surface, and solution conditions. The cantilever drive and setpoint imaging voltages were found to play a significant role in determining image quality and sample integrity. Slight deviations from the optimal setpoint drive and imaging voltages during data acquisition led to diminished resolution and, occasionally, sample etching. Accordingly, the choice of feedback conditions was based on optimized image quality.

All AFM images were acquired with a Digital Instruments "E" scanning head, which has a maximum lateral scan area of 14.6 μm $\times$ 14.6 μm. The crystals to be examined were transferred via pipette into a well that was defined by an O-ring placed on an AFM mount coated with a thin layer of vacuum grease. Once seated on the O-ring, the liquid cell has restricted lateral translation, making it important to minimize the need for tip positioning. Therefore, we devised the following procedure to reliably position the AFM tip over a crystal of interest. The cantilever was mounted in the AFM liquid cell and the laser spot was aligned on the cantilever tip in the absence of a sample surface. The liquid cell then was removed from the AFM optical head and replaced with the AFM mount containing the crystals of interest. Without adjusting the laser spot positioning screws and while monitoring the position of the laser spot through an optical microscope, the AFM optical head is translated in the *x-y* plane until the laser spot is located above a crystal of interest. The liquid cell containing the premounted cantilever tip is then reseated over the O-ring. This procedure also reduces the incidence of sample creep arising from relaxation of the O-ring.

Image analyses were performed on low-pass filtered AFM images, using Nanoscope III, version 4.22b1 (Digital Instruments), and National Institutes of Health Image, version 1.61 (National Institutes of Health; available by anonymous file transfer protocol from zippy.nimh.nih.gov), software packages.

Molecular modeling

Molecular models of the bovine and human insulin hexamers were generated in Quanta96 (Molecular Simulations, San Diego, CA), using the 2-Zn porcine insulin as an initial model. The crystal structure of this form was retrieved from the Brookhaven Protein Databank (Bernstein et al., 1977; Abola et al., 1987) as PDB entry code *pdb4ins.ent* (Baker et al., 1988). The structures of the modified insulin monomers were minimized using CHARMM by applying 50 steps of a modified Newton-Raphson minimization algorithm. The hexamers were then generated from the minimized structures with the appropriate symmetry operators. This minimization procedure allows for relaxation of any steric conflicts arising from the sequence alteration. The minimum energy structure of the 2-Zn porcine insulin hexamer was determined in the same manner to ensure that the calculated surface differences were not artifacts of the minimization procedure. Surface hydrophobicity and hydrophilicity were evaluated with

GRASP (Nicholls et al., 1991). All modeling was performed on a Silicon Graphics R3000 Elan workstation.

RESULTS AND DISCUSSION

Tapping-mode AFM imaging was performed directly under growth conditions in crystallization liquor on bunched aggregates of orthorhombic-shaped microcrystals of human and porcine insulins that were retrieved from prior crystallization in highly concentrated salt solutions (Schlichtkrull, 1956). Images were acquired on the most prominent face of a given microcrystal while growth was occurring on that face. These images revealed large micron-sized, molecularly flat terraces that were occasionally decorated with protein aggregates. Continued imaging revealed layer-by-layer growth, identical to previous observations in our laboratory for insulin crystals (Yip et al., 1996, 1998). AFM lattice images acquired on small regions of these terraces revealed molecular-scale contrast with nominal hexagonal order and two-dimensional lattice constants $a_1 = 49.0$ Å, $a_2 = 44.2$ Å, $a_3 = 49.0$ Å, $\gamma_{12} = 56°$, and $\gamma_{23} = 57°$ (Fig. 1). The vertical step height between individual terraces was ~30 Å, in good agreement with the thickness of the "donut-shaped" insulin hexamer (Baker et al., 1988). Inspection of the AFM images revealed that the terraces were translationally and rotationally commensurate, indicative of good crystal quality. These data are consistent with the close-packed hexagonal arrangement of insulin hexamers in the (001) plane of numerous insulin crystals that crystallize in the R3 space group (under conditions different from those of the ultralente forms) and have been structurally characterized by single-crystal x-ray diffraction. For example, the distance between neighboring hexamers in the (001) plane of the 2-Zn porcine insulin structure (space group: R3, $a = b = 82.5$ Å, $c = 35$ Å; $\alpha = \beta = 90°$, $\gamma = 120°$) is 46 Å, in excellent agreement with the two-dimensional lattice constants observed in the AFM data. Furthermore, 30-Å vertical separation between these terraces was in reasonable agreement with the c axis lattice parameter of the 2-Zn porcine insulin structure.

These data argue that human and porcine ultralente insulins crystallize in the trigonal crystal system, very likely as R3. This is supported further by a survey of the Brookhaven Protein Databank that revealed that ~65% of reported wild-type and analog insulin structures crystallized in the R3 space group, compared to only 2% of all registered diffraction structures.

In contrast to the porcine and human ultralente insulins, crystallization of bovine insulin under identical conditions yielded micron-sized irregular rhombohedral-shaped crystals with poorly defined crystal facets. Tapping-mode AFM performed under growth conditions in crystallization liquor revealed crystal growth modes and surface topographies that differed significantly from that observed for the human and porcine analogs (Fig. 2). Instead of hexagonal periodic contrast, the bovine crystal faces exhibited contrast that can be described best as bundles of parallel corrugated cylinders. The cylinders repeat at ~50-Å intervals, and the corrugations within a given cylinder repeat at ~45-Å intervals.

A more careful analysis of the data revealed slightly different lattice structures on different regions of a crystal. Lattice images acquired on region 1, on the surface of a small facet that emerges from the large face in Fig. 2 *A*, suggest a two-dimensional oblique unit cell with lattice constants of $a_1 = 40$ Å, $a_2 = 48$ Å, and $\gamma_{12} = 63°$ (Fig. 2 *B*). The oblique cell is a consequence of a lateral offset of adjacent cylinders. The large face that occupies most of the

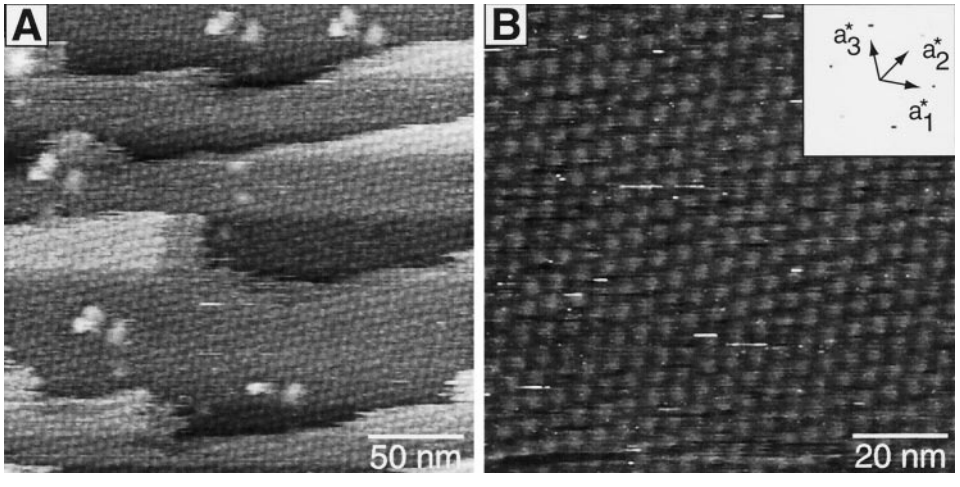

FIGURE 1 In situ tapping-mode AFM images of the (001) face of human insulin ultralente crystals acquired in crystallization liquor. (*A*) Large area scan revealing well-defined molecular terraces and translational and rotational commensurism between individual terraces. The vertical step height between terraces is ~30 Å. Scan rate: 2.0 Hz. (*B*) Lattice images revealing nominal hexagonal periodicity that is consistent with the expected hexamer packing motif on the (001) crystal plane of R3 porcine insulin. Scan rate: 2.0 Hz. (*Inset*) Two-dimensional Fourier power spectrum corresponding to real-space vectors: $a_1 = 49.0$ Å, $a_2 = 44.2$ Å, $a_3 = 49.0$ Å, $\gamma_{12} = 56°$, and $\gamma_{23} = 57°$, corresponding to lateral nearest-neighbor hexamer-hexamer contacts in the (001) R3 crystal plane (see Fig. 4). The AFM unit cell corresponding to the two-dimensional Fourier power spectrum is depicted by the solid white lines.

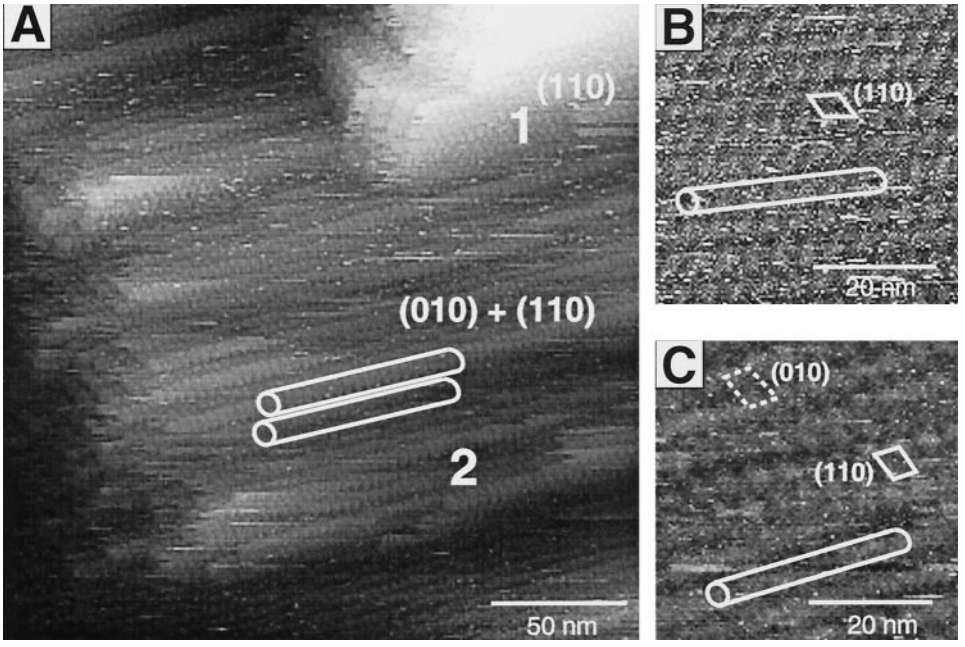

FIGURE 2 Tapping-mode AFM images of bovine insulin ultralente crystals acquired in crystallization liquor. Corrugated cylindrical features are evident on the large face. The cylinders are spaced at intervals of ~50 Å, and the interval between corrugations within a given cylinder is ~45 Å. Scan rate: 2.0 Hz. (*A*) Large area scan revealing corrugated row structures and a small crystal facet in the upper right-hand corner. (*B*) Data acquired on a small area of region 1 that reveals a unit cell with lattice constants $a_1 = 40$ Å, $a_2 = 48$ Å, and $\gamma_{12} = 63°$, consistent with packing of insulin hexamers on the (110) plane of the R3 structure. (*C*) Data acquired on a small area of region 2 revealing corrugated cylinders. Two distinct unit cells are evident in this region. The unit cell with lattice constants $a_1 = 48$ Å, $a_2 = 70$ Å, and $\gamma_{12} = 65°$, depicted by dashed white lines, is consistent with hexamer organization on the (010) plane. The second unit cell with lattice constants $a_1 = 43$ Å, $a_2 = 41$ Å, and $\gamma_{12} = 62°$, depicted by solid white lines, is consistent with the hexamer organization on (110).

image frame is somewhat rough, consisting of bunches of cylinders that emerge from kink sites on the crystal surface. Two different oblique unit cells were evident on various locations of this large face (region 2), one with lattice constants $a_1 = 43$ Å, $a_2 = 41$ Å, and $\gamma_{12} = 62°$, and the other with $a_1 = 48$ Å, $a_2 = 70$ Å, and $\gamma_{12} = 65°$ (Fig. 2 *C*).

The arrays of ordered corrugated cylinders observed in the lattice images of bovine ultralente insulin crystals and the measured lattice constants were consistent with the surface structure of R3 {hk0} planes, which contain close-packed stacks (i.e., cylinders) of "donut-shaped" insulin hexamers along the *c* axis (Figs. 3 and 4). More specifically,

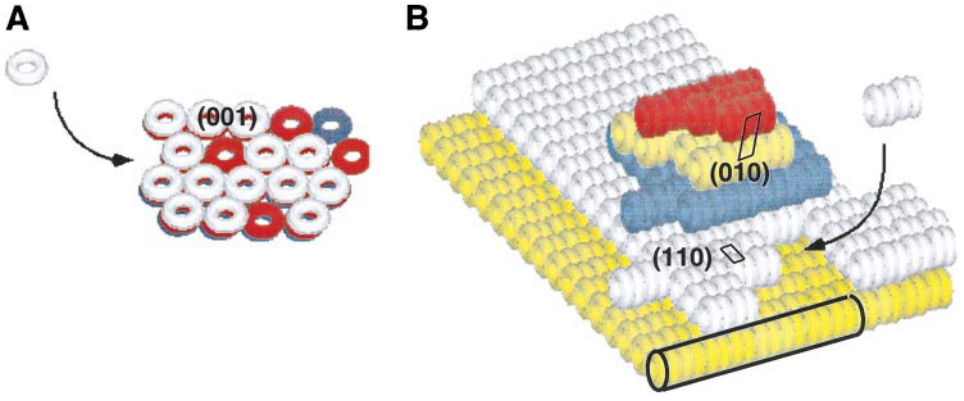

FIGURE 3 Schematic representation of the insulin hexamer packing on the prominent exposed crystal surfaces of (*A*) porcine (or human) insulin and (*B*) bovine ultralente insulin based on the R3 space group symmetry. In *A* the exposed surface is the (001) crystal plane, which is defined by close-packed hexagonal arrays of hexamers. This face, which predominates in porcine and human insulins, provides facile solvent access to the core of the insulin hexamer that contains the Zn^{2+} ion and to the solvent channels along the *c*-axis in the crystal. In *B*, the exposed surfaces correspond to the (010) and (110) crystal planes, which have close-packed stacks of insulin hexamers that hinder solvent access to the crystal. The arrows depict possible mechanisms of ultralente crystal growth, which may occur by attachment of single hexamers to growing (001) terraces (for human/porcine insulins in *A*) or by attachment of stacked hexamer aggregates to (010) or (110) planes (for bovine insulin in *B*).

these images reflect the organization of hexamers on the (010) and (110) planes in the 2-Zn porcine insulin. Comparison of the AFM data with the crystal structure suggests that the oblique unit cell from the AFM data acquired on region 1 can be assigned to hexamer organization on the (010) plane, whereas the observation of two lattices in region 2 can be attributed to a mixture of (010) and (110). The (010) unit cell surmised from the AFM data is oblique, unlike the rectangular cell defined by the *a* and *b* lattice vectors in the crystallographic model. Nevertheless, the oblique cell is a physically real representation of the hexamer organization on the (010) plane (Fig. 4 *B*). Similarly, the oblique unit cell observed by AFM assigned to (110) is one of two unit cell choices (the other being rectangular) that can be discerned from a normal view of this plane (Fig. 4 *C*).

The appearance of these oblique unit cells in the AFM data rather than the more obvious ones can be attributed to the unpredictable convolution of the AFM tip and sample during imaging, in this case resulting in the oblique cells dominating the force contrast and corresponding frequency components of the Fourier data. Despite this, the cylindrical features clearly indicate that the morphology of the bovine insulin crystals is dominated by (010) and (110) planes, and the lattice constants of the cells deduced from the Fourier analysis support these assignments. The occurrence of both planes in the same region is reasonable, as (010) and (110) have a common zone axis (the *c* axis), which is also consistent with the parallelism of the cylinders in region 2. Furthermore, the cylinders in region 1 are nominally parallel to those in region 2, arguing that the facet of region 1 grew from the large face in a commensurate manner. Interestingly, the insulin hexamers on the (010) and (110) faces are exposed "edge on" to the aqueous medium, in contrast to the (001) plane, which exposes the upper surface of the hexamers (Baker et al., 1988).

Crystal dissolution, which can influence pharmacokinetics, depends upon both the orientation of the constituent molecules on specific crystal planes and the relative exposed areas of these planes. The TMAFM images acquired in crystallization liquor indicated that human and porcine ultralente insulin crystals exhibited large (001) crystal terraces, whereas these planes were not evident for the bovine analog. This suggested that the facile dissolution of human and porcine ultralente insulin crystals may be attributed to the predominance of (001) crystal planes. The insulin hexamers are oriented on the (001) and (00$\bar{1}$) crystal planes such that the upper and lower surfaces of the hexamers are exposed (Figs. 3 and 4). This orientation would allow solvent to penetrate the crystal surface through the center of the hexamer, where Zn^{2+} ions reside, and through continuous interstitial solvent channels located between triads of insulin hexamer stacks (oriented along the *c* axis). In contrast, bovine ultralente crystals exhibited faces that were assignable to the densely packed (010) and (110) planes. The edge-on orientation of the hexamers on these crystal planes would inhibit solvent access to the individual hexamers; in particular, the centers of the hexamers and the solvent channels are not exposed on these surfaces. This restricted solvent access to these regions may account for the unique and more desirable basal time action of bovine ultralente. Although speculative, this argues that dissolution occurs via release of intact insulin hexamers rather than by dissociation of monomers.

All of the ultralente forms were prepared from identical crystallization liquors in this study, arguing against solvent-mediated crystallization effects. Although a high degree of sequence homology exists between bovine, porcine, and human insulins, key differences exist in the A-chain region (Table 1). In the human and porcine insulins, residues A8 and A10 are Thr and Ile, respectively, whereas in bovine insulin, these residues are replaced with Ala and Val. These sequence differences occur in a region of the insulin A-chain that is not involved directly in insulin monomer-monomer interactions. However, inspection of the R3 2-Zn porcine insulin structure revealed that this region is involved in hexamer-hexamer contacts between the upper and lower surfaces of the donut-shaped insulin hexamers as they stack along the *c* axis. Modeling of the bovine insulin hexamer reveals a twofold increase in exposed hydrophobic area compared to the porcine analog as a result of these sequence substitutions, with this increase confined entirely to the upper and lower surfaces of the insulin hexamer (Fig. 5). This is accompanied by a 25% reduction of the hydrophilic area on the same surfaces. This argues that formation of the hexamer stacks, which constitute the predominant (110) and (010) planes of the bovine ultralente crystals, is favored because of increased hydrophobic stabilization forces, an effect that is enhanced further by high salt concentrations during crystallization (Melander and Horvath, 1977). The morphology of the bovine ultralente crystals allows these hydrophobic regions to be buried beneath the surface of the (010) and (110) planes so as to avoid contact with the aqueous medium. This is reminiscent of observations for multimeric proteins, for which hydrophobic subunit patches typically are hidden at the interfaces between subunits and are not readily accessible to solvent (Lijnzaad and Argos, 1997). We note that the B30 residue in bovine and porcine insulins (Ala) differs from that of human insulin (Thr). This argues that the B30 residues, which are involved in interhexamer contacts in the (001) plane (Baker et al., 1988; Yip et al., 1998), do not play a significant role in determining the morphological properties of the ultralente insulins.

It is also reasonable to suggest that the increased hydrophobic character of the upper and lower surfaces of the bovine insulin hexamer favors a growth mechanism in which hexamers attach preferentially along the *c* axis. Insulin hexamers may organize preferentially into "short-stack" precrystalline aggregates to allow hydrophilic interactions between the edges of the insulin hexamer and the surrounding solvent while minimizing exposure of hydrophobic domains to the solvent (Fig. 3 *B*). In human or porcine insulins, the reduced hydrophobic character on the

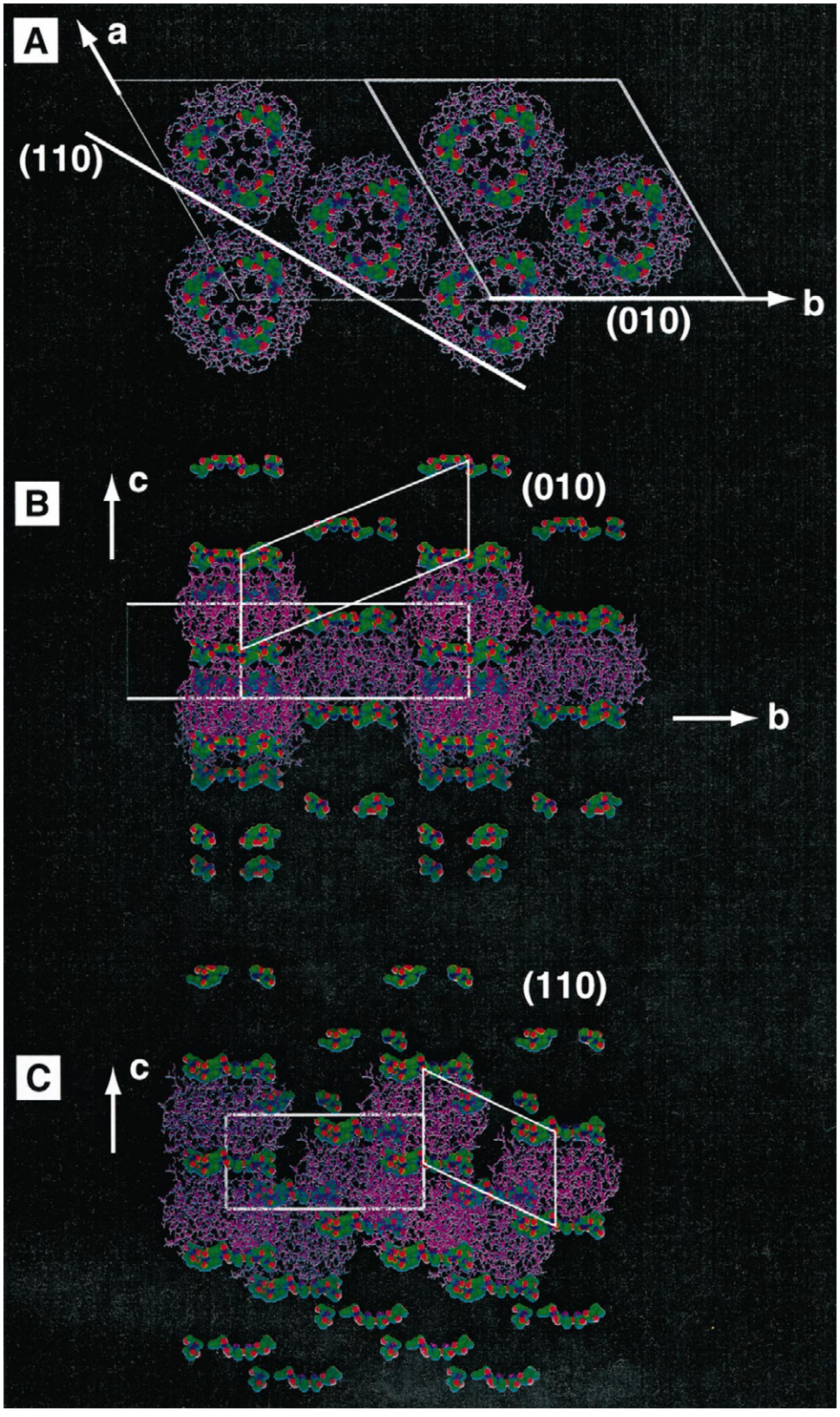

FIGURE 4 (*A–C*) Wireframe molecular models of the insulin hexamer packing in the R3 space group symmetry. Residues 8–10 of the A-chain are depicted as space filling. Only some of the hexamers have been drawn completely; the remaining ones are depicted only by the space-filled residues A8–A10. (*A*) Normal view of the (001) crystal plane illustrating the hexagonally ordered layer insulin hexamers. (*B, C*) View of the (*B*) (010) and (*C*) (110) planes, which contain cylindrical stacks of insulin hexamers laying in-plane with the edges of the hexamer exposed at the surface. Each face can be described by either a rectangular or an oblique unit cell, as depicted. The oblique cell on the (010) plane in *B* has lattice constants of 34.4 Å, 89.4 Å, and 60°, and the oblique cell on the (110) plane in *C* has lattice constants of 34 Å × 43 Å × 75°. These values agree reasonably with those deduced from the AFM data. The slightly smaller lattice constants measured by AFM can be attributed to intrinsic measurement error and to errors introduced from nonparallelism between the scanning tip and the crystal facet.

hexamer surface allows the lateral interhexamer contacts, which are hydrogen bonding and electrostatic in nature (Baker et al., 1988), to dominate, so that the hexamers assemble into the two-dimensional (001) layers rather than stacks (Fig. 3 *A*). This leads to large areas for the (001) faces of human and porcine insulin, as observed for numerous wild-type, recombinant, and analog insulins that crystallized in the R3 space group (Yip et al., 1996, 1997). The hydro-

TABLE 1 Amino acid sequences for bovine, human, and porcine insulins for residues 6–12 of the insulin A chain

A-chain residue number:	6	7	8	9	10	11	12
Bovine	Cys	Cys	**Ala**	Ser	**Val**	Cys	Ser
Human	Cys	Cys	**Thr**	Ser	**Ile**	Cys	Ser
Porcine	Cys	Cys	**Thr**	Ser	**Ile**	Cys	Ser

Those residues that differ are highlighted in bold.

phobic terms apparently dominate over these lateral interactions in bovine insulin crystallization such that growth of the (110) and (010) faces is favored over growth of the (001) layers.

The observed behavior suggests that, like pH and ionic strength (Durbin and Feher, 1996; Tiller, 1991), minor sequence changes can cause subtle changes in the free energy of hexamer attachment during crystallization. Similar observations were reported by us for the $Lys^{B28}Pro^{B29}$ insulin analog, which exhibited crystal growth characteristics that differed from native forms because of a sequence inversion in the B-chain (Yip et al., 1998). It has been suggested that protein-protein contacts in protein crystals involve exterior surfaces with compositions (aromatic C atoms, aliphatic C atoms, hydrogen bond donors, hydrogen bond acceptors) that are statistically identical to the rest of the protein surface, which led to the suggestion that protein-protein contacts were random and bear little resemblance to any specific recognition processes (Carugo and Argos, 1997). However, the observations here argue that the surface character and properties of the ultralente bovine and human/porcine hexamers are not statistically insignificant. On the contrary, these differences are sufficient to affect hexamer-hexamer association during crystallization and significantly alter crystal morphology.

It is well known that the conformation of the insulin hexamer depends on the crystallization conditions, with the individual monomers adopting one of three possible states: T-, R-, or R^f (Ciszak et al., 1995; Kaarsholm, 1989; Derewenda et al., 1989). In the T and R state monomers, the residues B1–B8 of the N-terminus of the insulin B-chain are in extended and α-helical conformations, respectively, whereas in the "frayed" α-helix or R^f monomer state, the α-helix is truncated, with residues B1 through B3 existing in an extended state. The T $\rightarrow$ R transition is induced by phenolic ligands that bind to hydrophobic pockets, thereby stabilizing the helical conformation of the B1–B8 residues. We cannot discern tertiary or secondary structure by AFM; therefore we cannot definitively assign a motif to the insulin monomers or the hexamer. However, the absence of phenolic ligands in the present study would suggest a T_6 hexamer, a conjecture supported by preliminary powder diffraction studies (G. D. Smith, personal communication).

The present study demonstrates that in situ AFM enables determination of molecular packing, space group symmetry, and interfacial structures of various crystalline ultralente insulin forms. Before the AFM studies described here, the small crystal dimensions and poorly defined crystal morphologies of ultralente insulin crystals precluded both crystal indexing and structure determination. Consequently, it has been difficult to elucidate the underlying reasons for the reputed different pharmacokinetics of the various ultralente formulations. Our TMAFM studies provide evidence that the different time actions of these formulations stem from morphology differences and the related packing and orientations of insulin hexamers at the crystal-solution interface, which can influence the contribution of microcrystal dissolution to the pharmacokinetics. Molecular modeling indicates that the upper and lower surfaces of the bovine insulin hexamer have greater hydrophobicity than those of its human and porcine counterparts, arguing that the unique morphology of the bovine form is a consequence of hydrophobically driven hexamer assembly. Such effects can have a significant impact on the physical properties and therapeutic efficacy of crystalline protein formulations.

We thank Dr. J. M. Beals, Dr. R. E. Chance (Eli Lilly and Company), and Dr. G. D. Smith (Hauptmann-Woodward Research Institute) for helpful discussions. We acknowledge the support of the Center for Interfacial Engineering at the University of Minnesota, a National Science Foundation Engineering Research Center. CMY acknowledges support of the Eli Lilly Postdoctoral Fellows program.

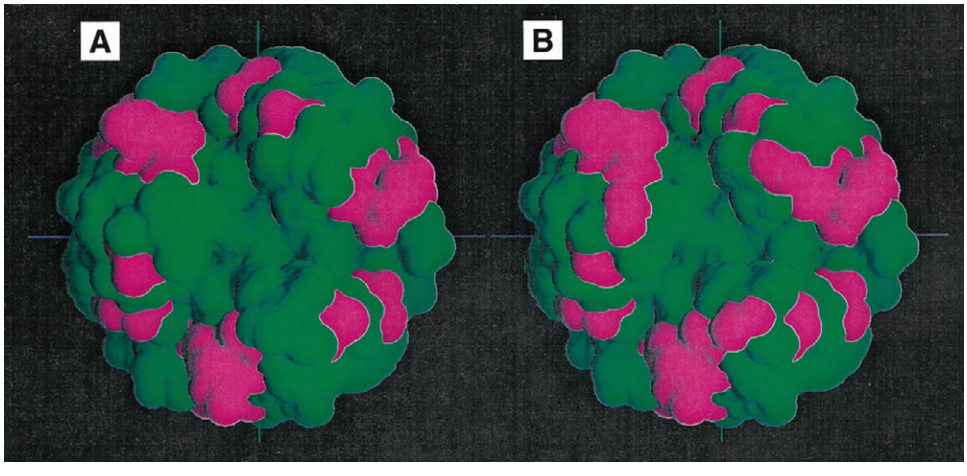

FIGURE 5 Molecular models of the surfaces of (*A*) porcine and (*B*) bovine insulin hexamers. These models depict exposed hydrophobic (*magenta*) and hydrophilic (*green*) regions as viewed down the threefold axis of the insulin hexamer along the *c* axis, looking into the center of the hexamers where the Zn^{2+} ions reside. The increase in hydrophobic character of the upper and lower surfaces of the bovine insulin hexamer in *B* is due to the replacement of the Thr and Ile residues at positions 8 and 10, respectively, of the porcine insulin A-chain, with Ala and Val.

REFERENCES

Abola, E. E., F. C. Bernstein, S. H. Bryant, T. F. Koetzle, and J. Weng. 1987. Protein Data Bank. *In* Crystallographic Databases—Information Content, Software Systems, Scientific Applications. F. H. Allen, G. Bergerhoff, and R. Sievers, editors. Data Commission of the International Union of Crystallography, Bonn, Cambridge, Chester. 107–132.

Baker, E. N., T. L. Blundell, J. F. Cutfield, S. M. Cutrfield, E. J. Dodson, G. G. Dodson, D. M. Crowfoot Hodgkin, R. E. Hubbard, N. W. Isaacs, C. D. Reynolds, K. Sakabe, N. Sakabe, and N. Vijayan. 1988. The structure of 2Zn pig insulin crystals at 1.5 Å resolution. *Philos. Trans. R. Soc. Lond. B.* 319:369–456.

Bernstein, F. C., T. F. Koetzle, G. J. B. Williams, Meyer, E. F., Jr., M. D. Brice, J. R. Rodgers, O. Kennard, T. Shimanouchi, and M. Tasumi. 1977. The Protein Data Bank: a computer-based archival file for macromolecular structures. *J. Mol. Biol.* 112:535–542.

Berson, S. A., and R. S. Yalow. 1966. Insulin in blood and insulin antibodies. *Am. J. Med.* 40:676–690.

Carter, P. W., A. C. Hillier, and M. D. Ward. 1994. Nanoscale surface topography and growth of molecular crystals: the role of anisotropic intermolecular bonding. *J. Am. Chem. Soc.* 116:944–953.

Carugo, O., and P. Argos. 1997. Protein-protein crystal-packing contacts. *Protein Sci.* 6:2261–2263.

Ciszak, E., J. M. Beals, B. H. Frank, J. Baker, C., N. D. Carter, and G. D. Smith. 1995. Role of C-terminal B-chain residues in insulin assembly: the structure of hexameric $Lys^{B28}Pro^{B29}$-human insulin. *Structure.* 3:615–622.

Derewenda, U., Z. Derewenda, E. J. Dodson, G. G. Dodson, C. D. Reynolds, G. D. Smith, C. Sparks, and D. Swenson. 1989. Phenol stabilizes more helix in a new symmetrical zinc insulin hexamer. *Nature.* 338: 594–596.

Durbin, S. D., and W. E. Carlson. 1992. Lysozyme crystal growth studied by atomic force microscopy. *J. Cryst. Growth.* 122:71–79.

Durbin, S. D., W. E. Carlson, and M. T. Saros. 1993. In situ studies of protein crystal growth by atomic force microscopy. *J. Phys. D Appl. Phys.* 26:B128–B132.

Durbin, S. D., and G. Feher. 1996., Protein crystallization. *Annu. Rev. Phys. Chem.* 47:171–204.

Galloway, J. A., and R. E. Chance. 1994. Improving insulin therapy: achievements and challenges. *Horm. Metab. Res.* 26:591–598.

Gammeltoft, S. 1988. Insulin Receptors, Part A: Methods for the Study of Structure and Function. Allan R. Liss, New York.

Graham, D. T., and A. R. Pomeroy. 1984. An in-vitro test for the duration of action of insulin suspensions. *Pharm. Pharmacol.* 36:427–430.

Hallas-Møller, K. Petersen, and J. Schlichtkrull. 1952. Crystalline and amorphous insulin-zinc compounds with prolonged action. *Science.* 116: 394–398

Haycock, P. 1983. History of insulin therapy. *In* Intensive Insulin Therapy. D. S. Schade, J. V. Santiago, J. S. Skyler, and R. A. Rizza, editors. Excerpta Medica, Amsterdam. 1–19.

Hillier, A. C., J. B. Maxson, and M. D. Ward. 1994. Electrocrystallization of an ordered organic monolayer: selective epitaxial growth of β-$(ET)_2I_3$ on graphite. *Chem. Mater.* 6:2222–2226.

Hillier, A. C., and M. D. Ward. 1994. Atomic force microscopy of the electrochemical nucleation and growth of molecular crystals. *Science.* 263:1261–1264.

Hollenberg, M. D. 1990. Receptor triggering and receptor regulation: structure-activity relationships from the receptor's point of view. *J. Med. Chem.* 33:1275–1281.

Kaarsholm, N. C., H.-C. Ko, and M. F. Dunn. 1989. Comparison of the solution structure flexibility and zinc binding domains for insulin, proinsulin and miniproinsulin. *Biochemistry.* 28:4427–4435.

Konnert, J. H., P. D'Antonio, and K. B. Ward. 1994. Observations of growth steps, spiral dislocations and molecular packing on the surface of lysozyme crystals with the atomic force microscope. *Acta. Crystallogr.* D50:603–613.

Kuznetsov, Y. G., A. J. Malkin, T. A. Land, J. J. DeYoreo, A. P. Barba, J. Konnert, and A. McPherson. 1997. Molecular resolution imaging of macromolecular crystals by atomic force microscopy. *Biophys. J.* 72: 2357–2364.

Land, T. J., A. J. Malkin, Y. G. Kuznetsov, A. McPherson, and J. J. DeYoreo. 1995. Mechanisms of protein crystal growth: an atomic force microscopy study of canavalin crystallization. *Phys. Rev. Lett.* 75: 2774–2777.

Land, T. J., A. J. Malkin, Y. G. Kutznesov, A. McPherson, and J. J. DeYoreo. 1996. Mechanisms of protein and virus crystal growth: an atomic force microscopy study of canavalin and STMV crystallization. *J. Cryst. Growth.* 166:893–899.

Last, J. A., and M. D. Ward. 1996. Electrochemical annealing and friction anisotropy of domains in epitaxial molecular films. *Adv. Mater.* 8:730–733.

Lijnzaad, P., and P. Argos. 1997. Hydrophobic patches on protein subunit interfaces: characteristics and prediction. *Proteins Struct. Funct. Genet.* 28:333–343.

Lyon, M. K., K. M. Marr, and P. S. Furcinitti. 1993. Formation and characterization of two-dimensional crystals of photosystem II. *J. Struct. Biol.* 110:133–140.

Malkin, A. J., Y. G. Kuznetsov, and A. McPherson. 1996. Defect structure in macromolecular crystals. *J. Struct. Biol.* 117:124–137.

Malkin, A. J., T. J. Land, Y. G. Kuznetsov, A. McPherson, and J. J. De Yoreo. 1995. Investigation of virus crystal growth mechanisms by in-situ atomic force microscopy. *Phys. Rev. Lett.* 75:2778–2781.

Mao, G., L. Lobo, R. Scaringe, and M. D. Ward. 1997. Nanoscale visualization of crystal habit modification by atomic force microscopy. *Chem. Mater.* 9:773–783.

McPherson, A., A. J. Malkin, Y. G. Kuznetsov, S. Koszelak. 1996. Incorporation of impurities into macromolecular crystals. *J. Cryst. Growth.* 168:74–92.

Melander, W., and C. Horvath. 1977. Salt effect on hydrophobic interactions in precipitation and chromatography of proteins: an interpretation of the lyotropic series. *Arch. Biochem. Biophys.* 183:200–215.

Muller, D. J., A. Engel, J. L. Carrascosa, and M. Velez. 1997. The bacteriophage phi29 head-tail connector imaged at high resolution with the atomic force microscope in buffer solution. *EMBO J.* 16:2547–2553.

Nicholls, A., K. Sharp, and B. Honig. 1991. Protein folding and association: insights from the interfacial and thermodynamic properties of hydrocarbons. *Proteins Struct. Funct. Genet.* 11:281.

Schabert, F. A., C. Henn, and A. Engel. 1995. Native *Escherichia coli* OmpF porin surfaces probed by atomic force microscopy. *Science.* 268:92–94.

Schlichtkrull, J. 1956. Insulin crystal II. Shape of rhombohedral zinc-insulin crystals in relation to species and crystallization media. *Acta Chem. Scand.* 10:1459–1464.

Smith, G. D., D. C. E. J. Swenson, G. G. Dodson, and C. D. Reynolds. 1984. Structural stability in the 4-zinc human insulin hexamer. *Proc. Natl. Acad. Sci. USA.* 81:7093–7097.

Tiller, W. A. 1991. The Science of Crystallization: Microscopic Interfacial Phenomena. Cambridge University Press, Cambridge.

Walz, T., P. Tittmann, K. H. Fuchs, D. J. Müller, B. L. Smith, P. Agre, H. Gross, and A. Engel. 1996. Surface topographies at subnanometer-resolution reveal asymmetry and sidedness of aquaporin-1. *J. Mol. Biol.* 264:907–918.

Yip, C. M., M. L. Brader, M. D. Ward, and M. R. DeFelippis. 1998. Atomic force microscopy of crystalline insulins: the influence of sequence variation on crystallization and interfacial structure. *Biophys. J.* 74:2199–2209.

Yip, C. M., and M. D. Ward. 1996. Atomic force microscopy of insulin single crystals: direct visualization of molecules and crystal growth. *Biophys. J.* 71:1071–1078.